

GIS-BASED LANDSLIDE SUSCEPTIBILITY MAPPING OF RONG RURAL MUNICIPALITY USING FREQUENCY RATIO METHOD



A Report

Submitted to

Rong Rural Municipality

Rong, Ilam, Nepal

By

Sagar Sitaula

M.Sc. 2nd semester

Reg-No.:5-2-0002-0345-2016

Central Department of Environmental Science

Tribhuvan University

Kirtipur, Kathmandu, Nepal

February 2023



TRIBHUVAN UNIVERSITY
Central Department of Environmental Science

Tel No: 4332147
Kirtipur
Kathmandu
Nepal

LETTER OF RECOMMENDATION

This is to certify that the Case study entitled “**GIS-based Landslide Susceptibility Mapping of Rong Rural Municipality Using Frequency Ratio Method**” carried out by **Mr. Sagar Sitaula**, as a partial fulfilment of the requirements for the award of Master’s Degree (M.Sc.) in Environmental Science has worked under my supervision and guidance.

I, therefore, recommend this case study for acceptance and approval.

.....

Supervisor

Prof. Dr. Sadhana Pradhanang
Central Department of Environmental science
Tribhuwan University
Kirtipur, Nepal



TRIBHUVAN UNIVERSITY
Central Department of Environmental Science

Tel No: 4332147
Kirtipur
Kathmandu
Nepal

LETTER OF APPROVAL

On the recommendation of supervisor “Dr. Sadhana Pradhanang”, this case study submitted by **Mr. Sagar Sitaula** entitled “**GIS-based Landslide Susceptibility Mapping of Rong Rural Municipality Using Frequency Ratio Method**” has been accepted and approved as the partial fulfillment of the requirement for the award of Master’s Degree (M.Sc.) in Environmental Science.

.....


Prof. Dr. Chhatra Mani Sharma
Head of the Department
Central Department of Environmental science
Tribhuvan University
Kirtipur, Nepal

ACKNOWLEDGEMENTS

The report entitled “**GIS-based Landslide Susceptibility Mapping of Rong Rural Municipality Using Frequency Ratio Method**” could not have been completed without the overwhelming cooperation and assistance of various persons and authority. I feel obliged to pay my sincere gratitude to them for the initiation, support, permission and guidance. I am thankful to Dr. Chhatra Mani Sharma, Head of the Department for his initiation and permission of this study. My sincere gratitude to my Supervisor Dr. Sadhana Pradhanang for her support, guidance and suggestions. I would always be in dept to Mr. Raju Chauhan for his valuable suggestions in the study accomplishment. I extend my heartfelt gratitude to my friends Niru Basnet, Somy Bhattarai, Rupesh Bohara, Sabin Rawal for their selfless assistance, their dedication, and their unwavering support. I would like to thank ICIMOD for providing the data required for the study. I would like to express my sincere appreciation to Rong Rural-Municipality for their generous financial assistance during my study. Their support has been instrumental in enabling me to pursue my academic goals and has helped alleviate some of the financial burdens associated with my research. I want to acknowledge my parents and lastly, I would acknowledge all those who directly and indirectly helped me in the course of study and report preparation.

Sagar Sitaula
2nd Semester
CDES
SN:1307

ABSTRACT

Landslides are one of the most common natural dangers in Nepal, inflicting significant loss of life and property every year in mountain, hilly, and Churia areas, particularly during the monsoon season. Landslides endanger not just the lives of the people who live in the area, but also the region's fragile biodiversity, which is not adequately protected. People in the region are largely impoverished and marginalized, making them more exposed to catastrophic occurrences such as landslides. The creation of a landslide hazard map is a critical first step in developing a safe preventative strategy and a good mitigation plan. The present study concentrates on the Landslide Susceptibility Mapping in the Churia area of Ilam district of Nepal by using Frequency Ratio method. For the study, landslides inventory was developed as well as eight landslide causative factors considered for study are slope, aspect, land use, road distance, curvature, geology, NDVI and river distance.

There were 105 landslides totaling 0.48 km², accounting for 0.30% of the overall research area. Following the creation of a susceptibility map, it was discovered that around 2.08% of the region is in the Very High zone, approximately 7.7% is in the High Susceptible zone, 24.6% is in the Moderate susceptible zone, approximately 39.1% is in the Low danger zone and 26.3% in very Low susceptible zone. Different factor maps were used to validate the map. The key variables responsible for landslides were discovered to include slope collapse owing to the unstable geology of the Churia region, river cutting, and the burden of large trees on the ground.

Human-induced landslides seems minimum; but, if human activity grows in the Churia region, there is a substantial risk of landslide occurrence because many landslides are weathered. Landslides have mostly harmed the forest biomass of the Churia area, and if due attention is not given, there is a risk of damage to human life, property, and the economy.

Keyword: *Landslide, Hazard, Map, Validate, Rong, Churia, Hazard Assessment, Susceptibility, frequency Ratio*

TABLE OF CONTENTS

LETTER OF RECOMMENDATION	ii
LETTER OF APPROVAL	iii
ACKNOWLEDGEMENT	iv
ABSTRACT.....	v
LIST OF TABLES	viii
LIST OF FIGURES	ix
ACRONMS AND ABBREVIATIONS	x
CHAPTER I: INTRODUCTION.....	1
1.1 Background.....	1
1.2 Statement of the problem	2
1.3 Objective.....	3
1.3.1 Specific objectives	3
CHAPTER-II: MATERIALS AND METHODES.....	4
2.1 Study Area	4
2.1.2 Geological Setting.....	5
2.2 Materials	5
2.3 Data Used.....	5
2.3.1 Primary data.....	5
2.3.2 Secondary data.....	5
2.5 Data Analysis	7
2.5.1 Landslide susceptibility mapping	7
3.5.2 Frequency ratio	7
CHAPTER-III: RESULT AND DISCUSSION.....	9

3.1 Landslide Inventory	9
3.2 Factor map of different aspect.	9
3.3 Landslide Causative factors	12
3.4 Landslide susceptibility Map	15
3.5 Discussion	17
CHAPTER-IV: CONCLUSION.....	20
Recommendations.....	20
References	22
ANNEXES	25
Annex 1: Landslide inventory co-ordinate	25
Annex 2: Very high susceptible landslide zones co-ordinate	27
Annex 3: High susceptible landslide zones co-ordinate	29

LIST OF TABLES

Table 1: Calculation table	12
----------------------------------	----

LIST OF FIGURES

Figure 1: Figure showing study area map.....	4
Figure 2: Flowchart of the methodology adopted for the study.....	8
Figure 3: Landslide inventory in the study area.....	9
Figure 4: Landslide causative factors used in the study (A) Aspect, (B) LULC, (C) NDVI, (D) Road distance, (E) Slope, (F) Stream distance (G) Curvature, (H) Geology.....	11
Figure 5: Relationship of landslides occurrences with the causative factors. (a) distance to stream (b) curvature, (c) aspect (d) slope (e) distance to road, (f) NDVI (g) geology, (h) LULC.....	14
Figure 6: Different factors and their prediction rate for landslide susceptibility.....	14
Figure 7: Distribution of landslides on different classes of susceptibility.....	15
Figure 8: Landslide susceptibility map of Rong rural municipality.....	16
Figure 9: Very high Landslides Susceptible Zones.....	17

ACRONYMS AND ABBREVIATIONS

Arc GIS	Aeronautical Reconnaissance Coverage Geographical Information System
CDES-TU	Central Department of Environmental Science, Tribhuvan University
DEM	Digital Elevation Model
FR	Frequency Ratio
GIS	Geographical Information System
GPS	Global Positioning System
Ha	Hectare
ICIMOD	International Centre for Integrated Mountain Development
Kml	Keyhole Markup Language
LS	Lower Siwalik
LULC	Land use and land cover
MBT	Main Boundary Thrust
MFT	Main Frontal Thrust
MS1	Lower Middle Siwalik
MS2	Upper Middle Siwalik
NDVI	Normalized Difference Vegetation Index
OLI	Operational Land Imager
SK	Sarung kh. Formation
SP	Shiprin Khola Formation
ST	Seti Formation
TK	Takure Formation
UI	Ulleri Formation
USGS	United States Geological Survey

CHAPTER I: INTRODUCTION

1.1 Background

The phrase "landslide" refers to a wide range of mass movements, including both rock avalanches and relatively sluggish soil slides. Typically happening on the surface of a rupture or on relatively thin zones of strong shear strain, a slide is a downward movement of soil or rock material (Varnes, 1996). Landslide is considered as a geological hazard; however, it has now become indispensable to study the landslide in a broad dimension of water science, earth science, engineering science, social science and culture, heritage and environmental science. In mountainous areas, landslides are a complicated geohazard that can have catastrophic effects on long-term socioeconomic development. Because of its rough topography, seismic activity, monsoon rains, and human activity on slope, Rong rural municipality is one of the most landslide-prone locations in the country. Additionally, this region lies in the southernmost mountain range of the Himalaya, Siwalik (Churia), and is made up of geologically extremely young sedimentary rocks such as mudstones, shale, sandstones, siltstones, and conglomerates and is delimited by MFT in the south and Main Boundary Thrust (MBT) in the north (Dhakal, 2014; Bhandari & Dhakal, 2014).

These are soft, unconsolidated rocks that disintegrate readily. As a result, the geology of this range is extremely weak and brittle. As a result, the Siwalik range is growing increasingly vulnerable to slope collapse. This region is frequently and severely affected by landslides in the past, and prone to more landslides induced devastations in the future. Despite the potential for dangerous landslides in the area, the majority of the region lacks landslide susceptibility maps that may be used to analyze and reduce the risk of landslides.

A number of techniques and technologies may be used to locate and map slides. The most extensively used technique to locate and map landslides historically has been visual interpretation of stereoscopic aerial photos (Turner & Schuster, 1996). Aerial photography or remote-sensing photos that show the topographical expression of the landslide are often used to map the surface area impacted by the slide. Surface observations and measurements must be reinforced by reconnaissance at depth if the landslide is old or inactive because erosion may have deteriorated its morphological characteristics and boundaries (Dikau et al., 1996). Analyzing the distribution and frequency of previous landslides is necessary to pinpoint locations at increased risk of landslides. With the use of remote sensing and Geographic Information System (GIS) capabilities, historical

landslides may be mapped (Audisio et al., 2009; Mandal & Mondal, 2019; Yalcin, 2008; Yalcin et al., 2011; Yilmaz & Keskin, 2009). To identify a region's landslide susceptibility, provide the scientific data necessary for its prevention and to better anticipate where, when, and how frequently landslides will occur in a given location quantitative spatial analysis can be utilized (Yilmaz, 2009).

Landslide Susceptibility (LS) is an assessment that quantifies the volume or area and the spatial probability of a landslide event by providing a relative estimation of the spatial events of landslides in a mapping unit based on the conditions of local terrain, and it may also include information about the temporal probability of the expected landslide event, the intensity and velocity rates of existing or potential landslide events, and the intensity and velocity rates of existing or potential landslide events (Fell et al., 2008; Guzzetti et al., 1999; Lepore et al., 2011; Rossi & Reichenbach, 2016). The statistical model was used for this study because it has been widely used to examine LS by merging and integrating statistical models with geographical data and GIS applications. The main concept is to use the information in conjunction with geo-environmental conditioning variables to extract the amount of detail provided by the landslide data itself in order to determine landslide susceptibility in the research region. A bivariate statistical approach known as the Frequency Ratio (FR) was used in this research to generate a landslide susceptibility map for Rong Rural Municipality, Province-1, Nepal.

1.2 Statement of the problem

Nepal is one of Asia's most prone countries to landslides (OCHA, 2020). The nation is geologically young and still changing, having formed as a consequence of tectonic uplift of sedimentary deposits. The rock-mass in the Himalaya has a high degree of fragility and a greater proclivity to undergo fast disintegration under the influence of climatic variables. Landslides cause enormous damage, including: loss of human life, destruction of crops, loss of top soil, destruction of natural vegetation, destruction of buildings and property, interference with cultural sites, and thus affecting community lives and people's daily life, as well as negatively affecting the quality of water in rivers or streams (Schuster, 1996). About 12,000 small and large-scale landslides occur in Nepal every year, most of which often remain unnoticed and unreported mainly because of an inadequate information system, little economic impact, or little harm to humans and national infrastructure {Bhattarai et al (2002) as mentioned in Lamichhane and Bhattarai (2019)}.

The major purpose of this study is to examine the mapping of landslide susceptibility in the Churia area of Rong rural-municipality. Because this region has not been researched in terms of landslide susceptibility assessments, this study will provide information on landslide susceptibility, vulnerability, and risk, as well as aid in the implementation of preventative and mitigating measures. Landslide susceptibility study and management at the regional and local levels are critical. A landslide susceptibility map can help in estimating, managing, and mitigating landslides. This research will help to advance the methodological approach to landslide susceptibility modeling in a comparable location. This study will also determine landslide susceptibility, which will be useful in limiting the impact of landslides on life, property, and development in the Churia region of Rong rural-municipality. Planners and engineers might benefit from landslide susceptibility maps for development activities and land-use planning. Not only that, but this study has been beneficial to the Rong rural-municipality as well as the knowledge of many elements of landslides. To address the landslide problem in the Churia area of Rong rural-municipality by creating a landslide inventory map that includes detailed information about the landslide's location, type, topography, forest type, land-use and land-cover vegetation condition, geography, and other risk elements. This will aid in the planning, development, and strategy-making processes for landslide hazard management.

1.3 Objective

The general objective of the study is to make the landslide susceptibility mapping of Rong Rural-Municipality.

1.3.1 Specific objectives

- To make the landslide inventory of Rong Rural Municipality.
- To assess the landslide hazard susceptible zones in Rong Rural Municipality.
- To study the role of various parameter of landslide in study area.

CHAPTER-II: MATERIALS AND METHODES

2.1 Study Area

The study area is located in Eastern Chure Region of Rong rural-municipality, Ilam (Figure 1). This municipality is located in the southern part of Ilam district bordering Jhapa District. This is a hilly municipality having steep and sloppy Terrain. Maize, wheat and paddy are the major cereals and Mustard, Sugarcane, Ginger, Turmeric are the major cash crops produced in this place. Landslide and soil erosion are the serious hazards seen in this region. The study site has the tropical climate where the rainy season starts from June and ends in September. The average temperature in the study area ranges from 19°C to 31°C.

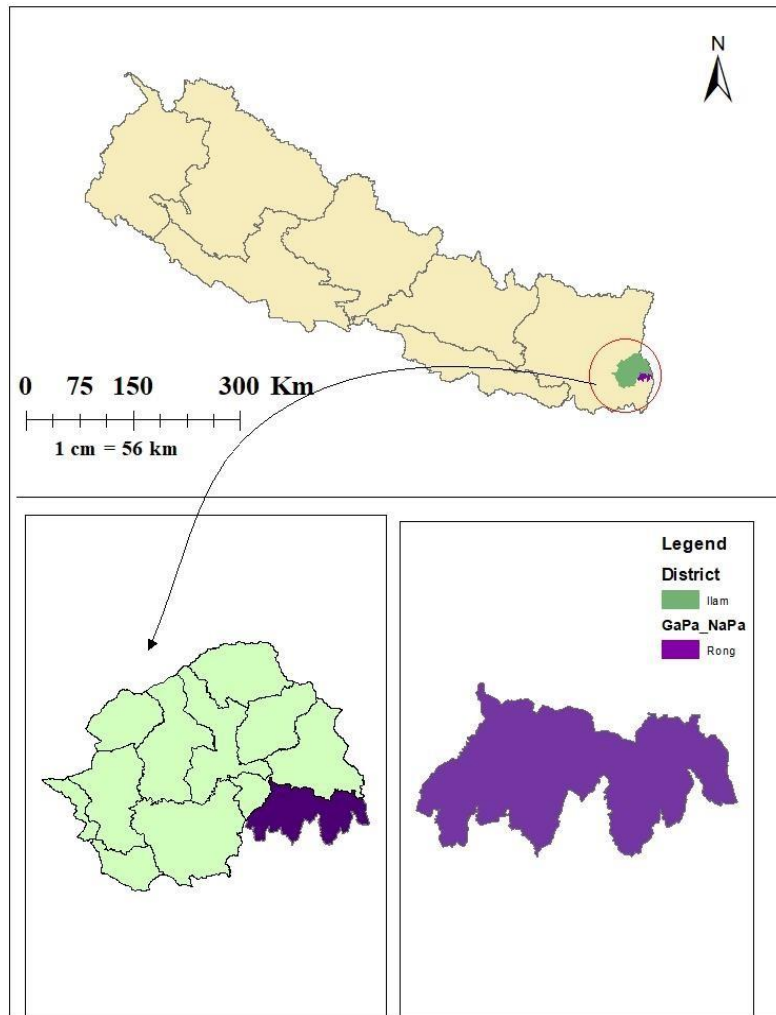


Figure 1: Figure showing study area map

2.1.2 Geological Setting

The Nepal Himalaya is separated into five major geological and tectonic zones: Terai (Indo-Gangetic plain), Sub Himalaya (Siwalik), Lesser Himalaya, Higher Himalaya, and Tibetan-Tethys Himalaya (Upreti, 1999; Gansser, 1964).

The research region is mostly located in the Siwalik zone, with a component in the lower part of the Lesser Himalaya, and is composed of geologically extremely young sedimentary rocks such as mudstones, shale, sandstones, siltstones, and conglomerates. These are soft, unconsolidated rocks that disintegrate readily.

Tectonically, this siwalik region is delimited in the south and north by the Himalayan Frontal Thrust (HFT) and the Main Boundary Thrust (MBT). The landscape transforms from mild to steep, and a pressure ridge may be seen. Geologically, the research area includes rocks from the midland group as well as newer deposits. Lower Siwalik, Middle Siwalik, and Upper Siwalik are the three classes of Siwalik, which are followed by Takure formation, Syangja formation, and Seti formation. The Lower Siwalik is made up of unevenly laminated strata of fine-grained greenish sandstone and siltstone with mudstone, according to (Dhakal, 2015). Fine to extremely coarse-grained sandstone and pebbly sandstone interbedded with mudstone and siltstone characterize the Middle Siwalik (Bhandari & Dhakal, 2019; Dhital, 2015). Likewise, the recent deposit is made up of alluvium, boulders, gravels, sands, and clays.

2.2 Materials

ArcGIS pro Software, Satellite data, DEM, Remote sensing tool and field survey tools

2.3 Data Used

2.3.1 Primary data

Primary data were obtained in the field using tools such as GPS and a checklist. To collect data for the study, three field surveys were done. The first preliminary field visit was held from the 20th of October, 2022, during which the research area was briefly investigated and ideas about the study area were acquired to facilitate the second phase field visit. The second phase field visit was held from 17th to 21st, December 2022, and was focused on primary data collecting and validation for landslide inventory.

2.3.2 Secondary data

The geological map was obtained from the Government of Nepal's Department of Mines and Geology (DMG). The geology of the study region was studied using a geological map with a scale of 1:250,000. Before verifying the landslide, Google Earth Imagery was utilized to indicate the landslide polygon in the desk. It was also utilized to create the validated landslide polygon and for additional research. For the analysis, historical time-based pictures from Google Earth were employed. The factor maps were created using a 12.5 m DEM acquired from the Alaska satellite facility.

2.4 Methods

The study was based on geospatial application and field survey. The landslide inventory of the study area was made from the observation of pervious landslides in the study area from satellite data and field observation. Then the susceptible zones of landslide were assessed in further process. The different factors that are possible and potential to cause landslide event was selected. The factors such as elevation, slope, aspect, geology, distance to stream, normalized difference vegetation index (NDVI), distance from road, curvature, land use and land cover (LULC) etc. was analyzed. Based on the interpretation of satellite images, remote sensing data, and GIS, both primary and secondary data were collected to construct the spatial inventory map and the landslide susceptibility map. Several theme data layers representing landslide conditioning elements were produced for the construction of the thematic data layer. The land cover of the study area was also thoroughly analyzed for the selection of highly susceptible zone of landslide in the Rong rural municipality.

Different methods were used for hazard mapping by analyzing the data obtained from field and desk. Visual interpretation and digitization of landslides over satellite pictures taken in Google Earth from 2018 to 2023 (January, 2018) were employed to remotely update the landslide inventory. The landslide was marked by creating polygons and then loaded into Arc GIS software for future research. The polygon shape landslide was transformed into raster data and the projection was WGS 1984 UTM zone 45 N. A total of 105 landslides were detected and mapped, 20% of the digital inventory landslides were strongly confirmed by field surveys, and these landslide polygons were mapped for the inventory. Various factors, ArcGIS pro software, DEM and other data are utilized for the final preparation of landslide susceptibility map.

2.5 Data Analysis

The data gathered was examined using statistical techniques in MS-Excel and ArcGIS pro. The findings were compiled and presented in tables, and different hazard and susceptibility maps were created.

2.5.1 Landslide susceptibility mapping

The Frequency Ratio Model (FR) was used to predict landslide vulnerability. The susceptibility and analysis of landslides entails a variety of procedures and approaches. It takes into account the inherent elements that make the region prone to landslides. A base map and a factor map are required for landslide susceptibility analysis. As a base map, the Landslide Inventory map was utilized. This study took into account intrinsic elements such as slope, aspect, curvature, NDVI, geology, distance from road, distance to streams and land cover. The parameters were completely chosen based on their efficacy and availability. The intrinsic components are chosen during a detailed field visit. Total of eight factors were used to generate the landslide susceptibility map. These factor maps and base maps were used to generate landslide susceptibility map for the study area. The Digital Elevation Model was used to create every factor map such as slope, aspect, Elevation, and curvature (DEM). Similarly, a land cover map was obtained using land cover satellite data. The geological map was created using the Department of Mines and Geology's georeferenced map.

3.5.2 Frequency ratio

To obtain the frequency ratio (FR) for each class of the causative factors, a combination has been established between the landslide inventory map and factor map using the Eq. (1) (Mondal & Maiti, 2013).

$$Fr = \frac{Npix(1)/Npix(2)}{\sum Npix(3) / \sum Npix(4)} \quad (1)$$

N pix (1) = The number of pixels containing landslide in a class

N pix (2) = Total number of pixels of each class in the whole area

\sum N pix (3) = Total number of pixels containing landslide

$\sum N \text{ pix (4)} = \text{Total number of pixels in the study area}$

The derived frequency ratio is summed to develop a Landslide Susceptibility Index (LSI) map using Eq. (2) (Lee & Talib, 2005).

$$LSI = Fr_1 + Fr_2 + Fr_3 + Fr_4 + \dots + Fr_n \quad (2)$$

where Fr is the frequency ratio, and n is the number of selected causative factors.

According to the technique, the ratio is that of the area where the landslides is occurred, to the total area, so that the value of 1 is an average value. If the value is greater than 1, it means the percentage of the landslide is higher than the area and indicate a higher correlation, whereas values lower than 1 indicate a lower correlation (Akgun et al.,2007). The LSI map is reclassified to develop a landslide susceptibility map. The methodology adopted for the study is shown in Figure 2.

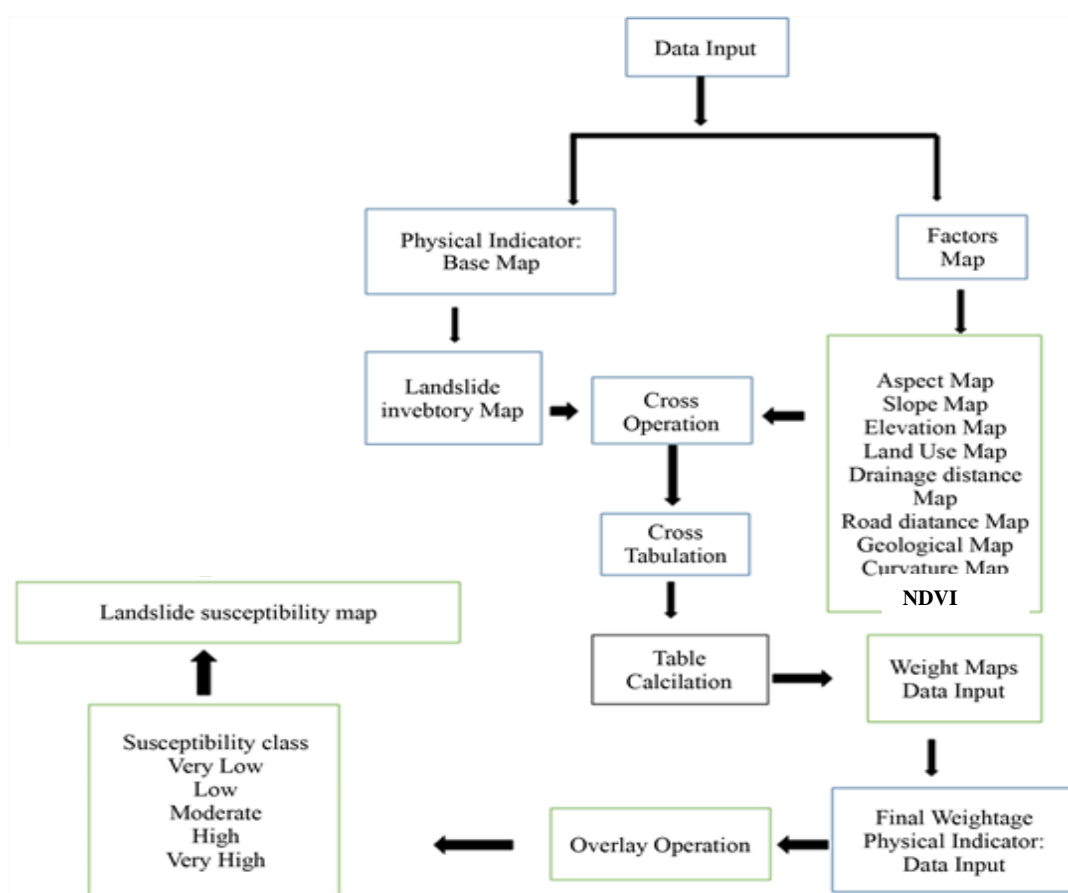


Figure 2: Flowchart of the methodology adopted for the study

CHAPTER-III: RESULT AND DISCUSSION

3.1 Landslide Inventory

Based on the ALOS PALSAR RTC 12.5m DEM and field visits, 105 landslides with a total area of 0.48 km sq were mapped (Fig. 3). The area's rock slides are caused mostly by geological discontinuities along joints, fractures, bedding planes, and severe topographical gradients. Heavy rains and slope are the primary causes of debris flow. Rotational landslides are mostly caused by toe erosion and undercutting of recent terraces.

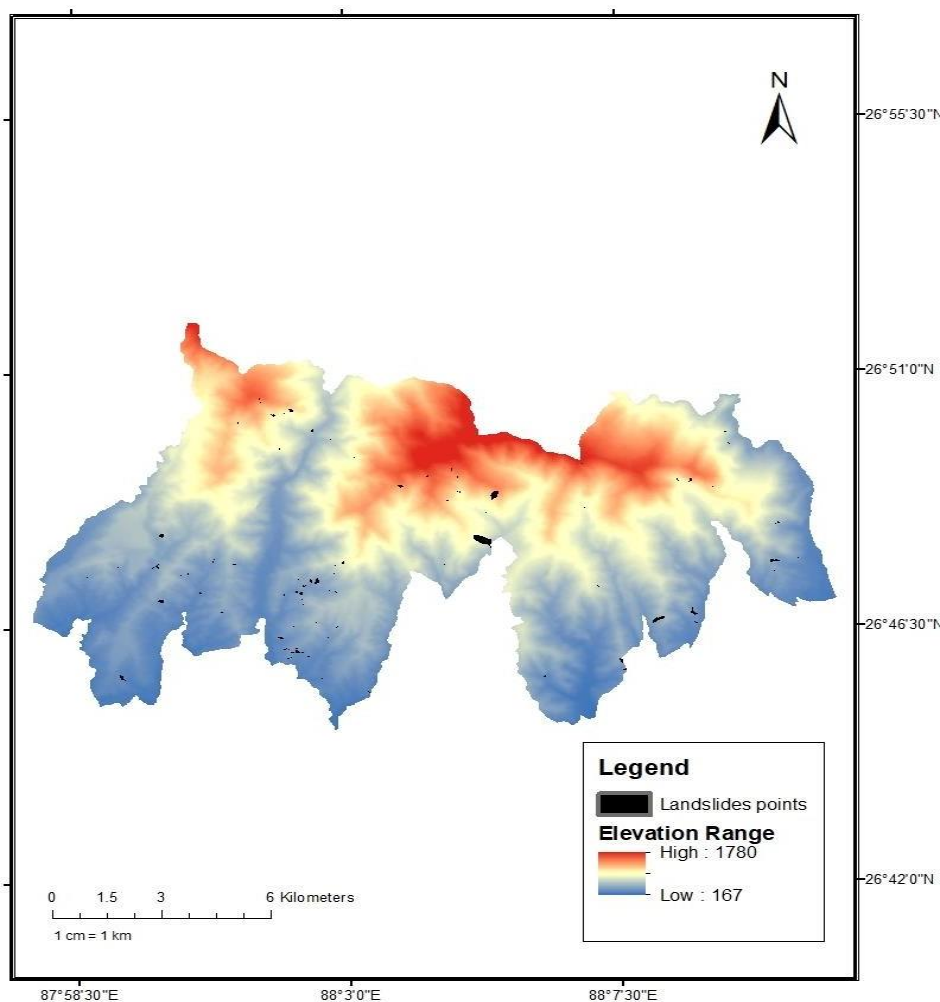
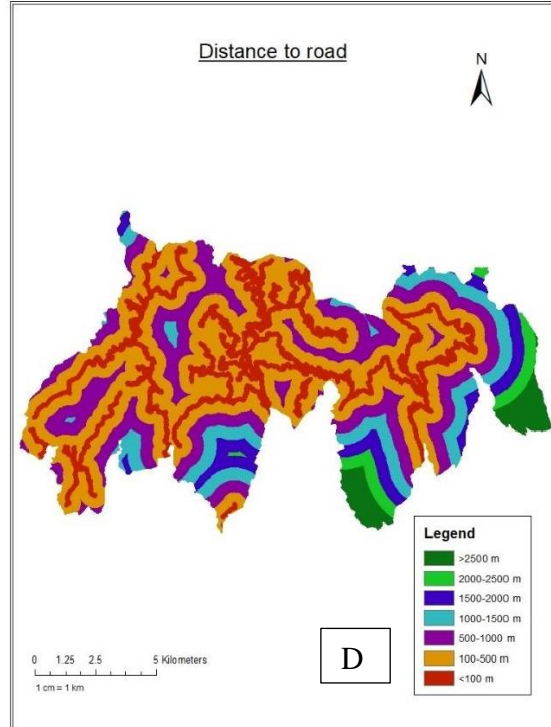
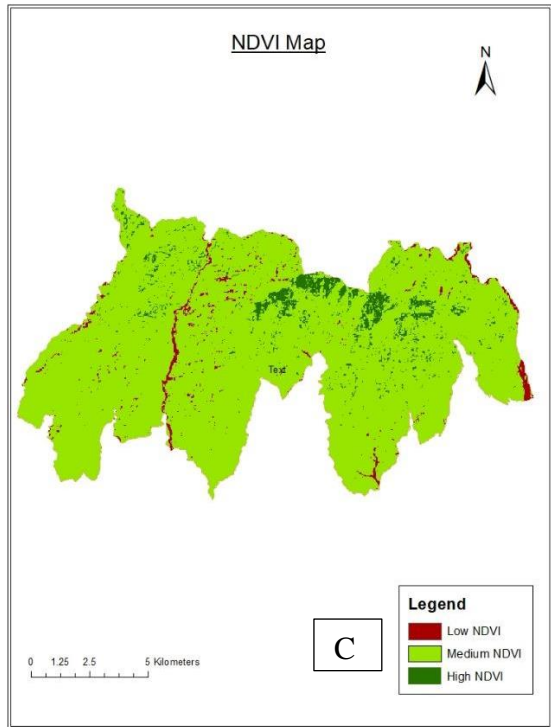
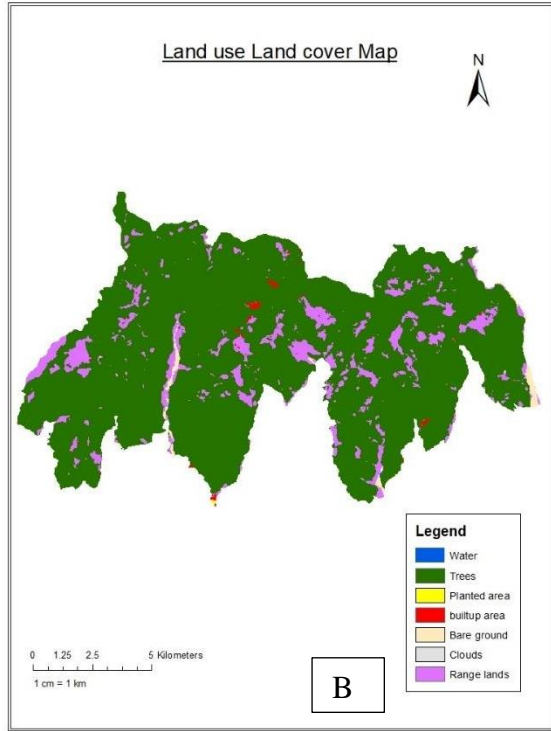
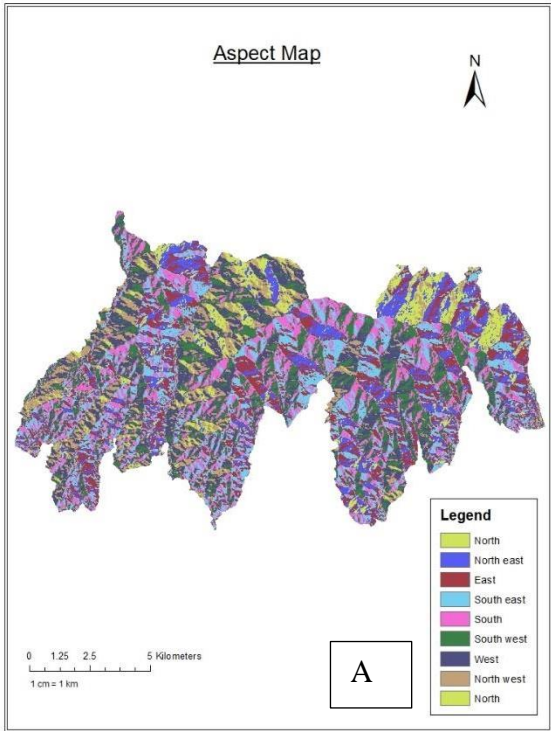


Figure 3: Landslide inventory in the study area

3.2 Factor map of different aspect.

Eight different factor maps were created and their range of susceptibility for landslide was identified and employed for the preparation of final landslide susceptible zones in the study area.



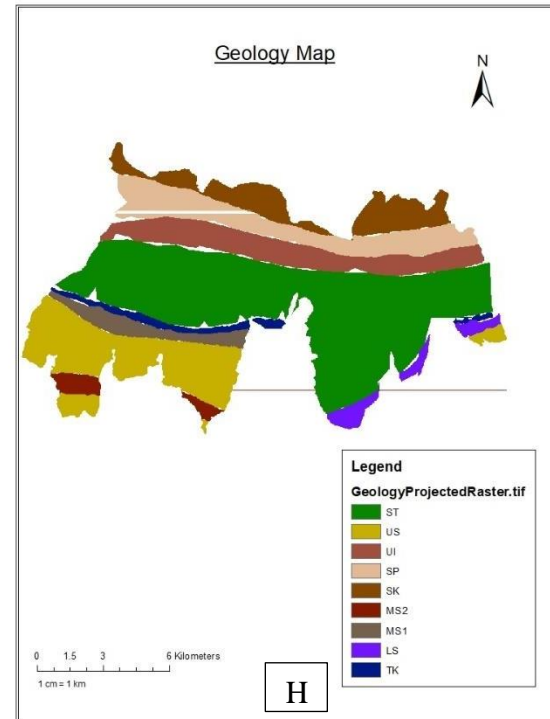
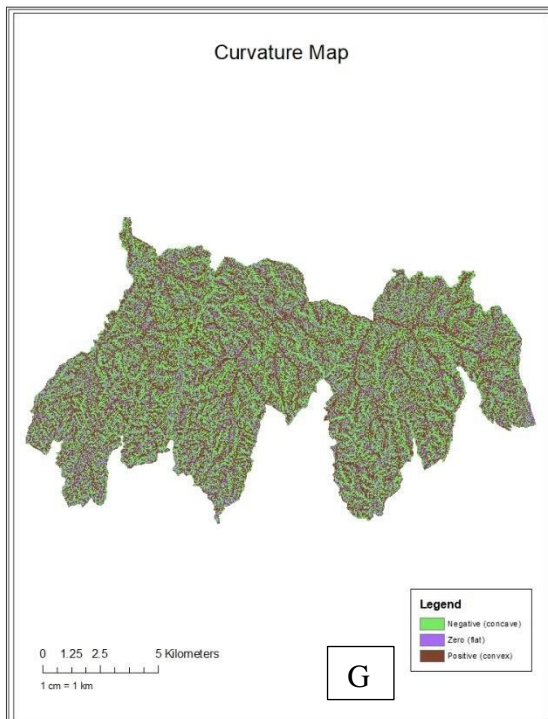
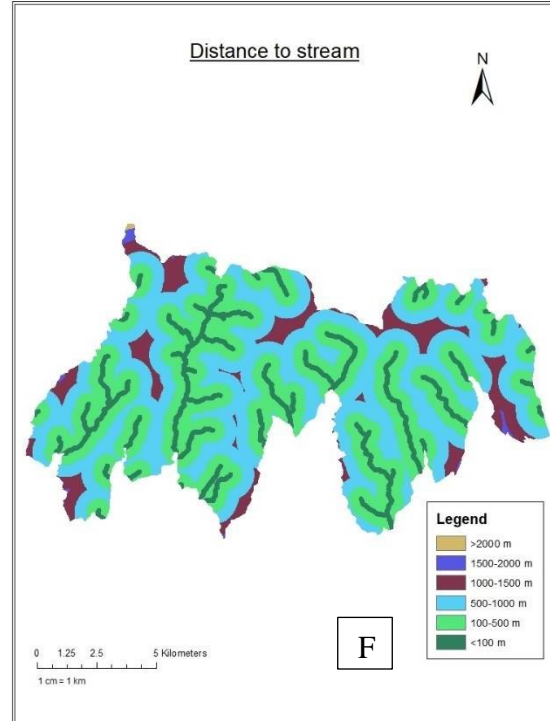
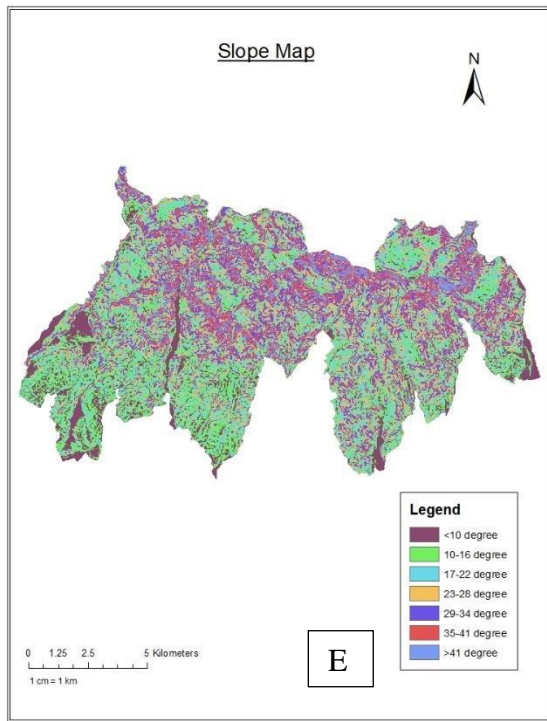


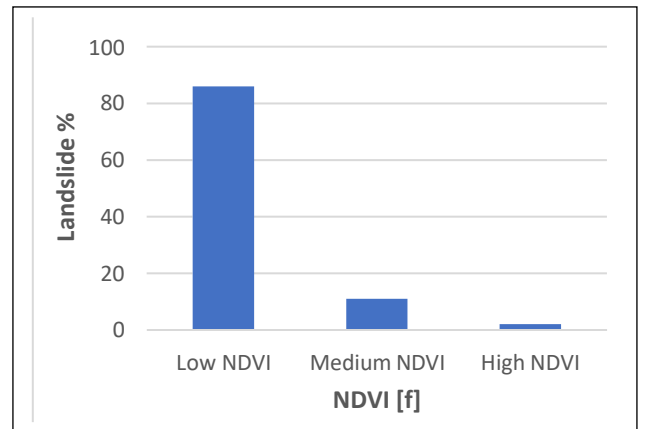
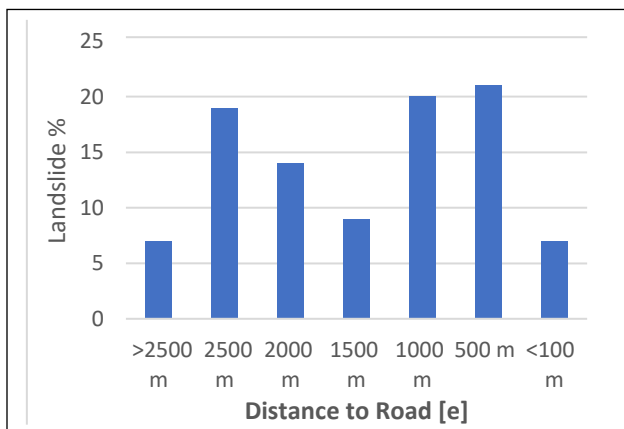
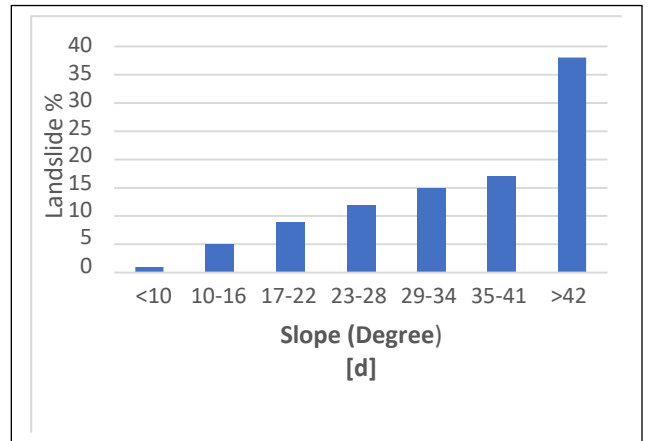
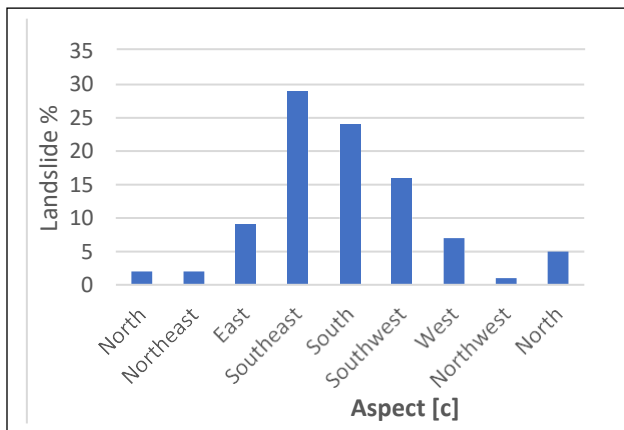
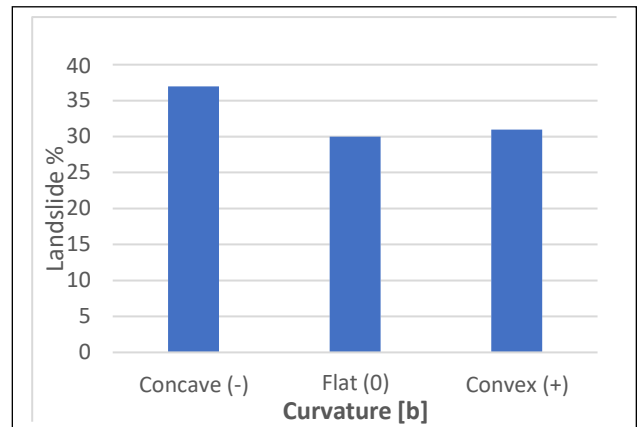
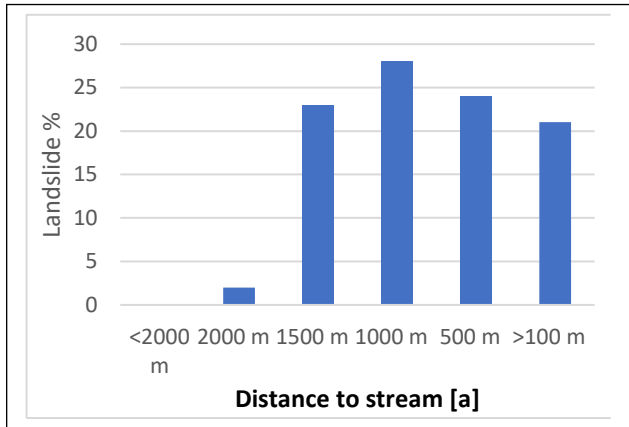
Figure 4: Landslide causative factors used in the study (A) aspect, (B) LULC, (C) NDVI, (D) Road distance, (E) Slope, (F) Stream distance (G) curvature, (H) Geology.

3.3 Landslide Causative factors

The study's causal variables are listed in Table 1, and the weight they carry are calculated to each type of causal factors.

Table 1: Calculation table

Parameters	Classes	Class Pixel	%class Pixels	Landslide Pixels	%Landslide Pixel	Frequency Ratio (FR)	Relative Frequency (RF)	Prediction Rate (PR)
Slope	<10 degree	102837	10.48687267	53	1.767255752	0.000515379	0.019017664	5.498839845
	10-16 degree	169156	17.24979758	249	8.302767589	0.001472014	0.05431786	
	17-22 degree	212938	21.71449666	545	18.17272424	0.00255943	0.094443928	
	23-28 degree	198715	20.26409661	660	22.00733578	0.00332134	0.122558657	
	29-34 degree	166359	16.96457161	691	23.04101367	0.004153668	0.15327187	
	35-41 degree	97533	9.945993682	455	15.17172391	0.004665088	0.172143458	
	>42 degree	33088	3.374171193	346	11.53717906	0.010456963	0.385865803	
Total		980626		2999		0.027143881		
Parameters	Classes	Class Pixel	%class Pixels	Landslide Pixels	%Landslide Pixel	FR	RF	PR
Curvature	Concave (-)	396607	40.14114942	1353	44.68295905	0.003411438	0.377747483	1.103772148
	Flat (0)	192250	19.4578915	528	17.43725231	0.002746424	0.304110722	
	Convex (+)	399174	40.40095908	1147	37.87978864	0.002873434	0.31817447	
Total		988031		3028		0.009031295		
Parameters	Classes	Class Pixel	%class Pixels	Landslide Pixels	%Landslide Pixel	FR	RF	PR
Aspect	North	40774	4.157956244	19	0.633544515	0.000465983	0.020963889	4.168390751
	Northeast	100494	10.24794366	58	1.933977993	0.000577149	0.025965066	
	East	140414	14.31881268	311	10.37012337	0.002214879	0.09964409	
	Southeast	149835	15.27952553	980	32.67755919	0.006540528	0.294248576	
	South	138959	14.17043807	759	25.30843615	0.005462043	0.24572914	
	Southwest	152727	15.57443918	563	18.77292431	0.003686316	0.165841852	
	West	134484	13.71409691	238	7.93597866	0.001769727	0.079617384	
	Northwest	89088	9.084809091	32	1.067022341	0.000359195	0.016159664	
	North	33851	3.451978634	39	1.300433478	0.001152108	0.051831607	
Total		980626		2999		0.022227928		
Parameters	Classes	Class Pixel	%class Pixels	Landslide Pixels	%Landslide Pixel	FR	RF	PR
Stream	<2000 m	501	0.050706911	0	0	0	0	1
	2000 m	3813	0.385919065	1	0.033025099	0.000262261	0.021860522	
	1500 m	87627	8.868851281	243	8.025099075	0.002773118	0.231150944	
	1000 m	394213	39.89884933	1349	44.55085865	0.003422008	0.285238635	
	500 m	403084	40.79669565	1176	38.83751651	0.002917506	0.243186299	
	>100 m	98793	9.998977765	259	8.553500661	0.002621643	0.218524901	
Total		988031		3028		0.011996536		
Parameters	Classes	Class Pixel	%class Pixels	Landslide Pixels	%Landslide Pixel	FR	RF	PR
Road	>2500 m	37948	3.840770178	55	1.816380449	0.001449352	0.077922137	2.0758182
	2500 m	27179	2.75082462	97	3.20343461	0.003568932	0.191878059	
	2000 m	53903	5.455598053	148	4.887714663	0.002745673	0.147616816	
	1500 m	93079	9.42065583	159	5.250990753	0.001708226	0.091840126	
	1000 m	213848	21.6438553	811	26.78335535	0.003792413	0.203893188	
	500 m	383814	38.84635199	1514	50	0.003944619	0.212076291	
	<100 m	178260	18.04194403	244	8.058124174	0.001368787	0.073590708	
Total		988031		3028		0.018578002		
Parameters	Classes	Class Pixel	%class Pixels	Landslide Pixels	%Landslide Pixel	FR	RF	PR
NDVI	Low NDVI	23448	2.373334602	491	16.28524046	0.020939952	0.861371955	12.50408639
	Medium NDVI	922149	93.33709186	2496	82.78606965	0.002706721	0.111341873	
	High NDVI	42380	4.289573543	28	0.928689884	0.00060689	0.027177664	
Total		987977		3015		0.024307362		
Parameters	Classes	Class Pixel	%class Pixels	Landslide Pixels	%Landslide Pixel	FR	RF	PR
Geology	ST	404706	42.18746091	1324	48.21558631	0.003271511	0.136597523	3.614539156
	US	156778	16.34289026	437	15.91405681	0.002787381	0.116383335	
	UI	107081	11.16236355	387	14.09322651	0.003614087	0.150901317	
	SP	104503	10.89362705	253	9.213401311	0.002420983	0.101084891	
	SK	86223	8.988078857	7	0.254916242	8.11848E-05	0.003389763	
	MS2	18989	1.979455939	3	0.109249818	0.000157986	0.006596501	
Parameters	Classes	Class Pixel	%class Pixels	Landslide Pixels	%Landslide Pixel	FR	RF	PR
LULC	Water	299	0.030262668	0	0	0	0	9.92016472
	Dense trees	876081	88.67073003	1450	48.07692308	0.001655098	0.014862724	
	Planted crops	196	0.019837735	0	0	0	0	
	Builtup area	3039	0.307586112	229	7.592838196	0.075353735	0.676673953	
	Bare ground	8509	0.861220871	195	6.465517241	0.022916912	0.205793079	
	Clouds	5	0.000506065	0	0	0	0	
Total		988016		3016		0.111358664		



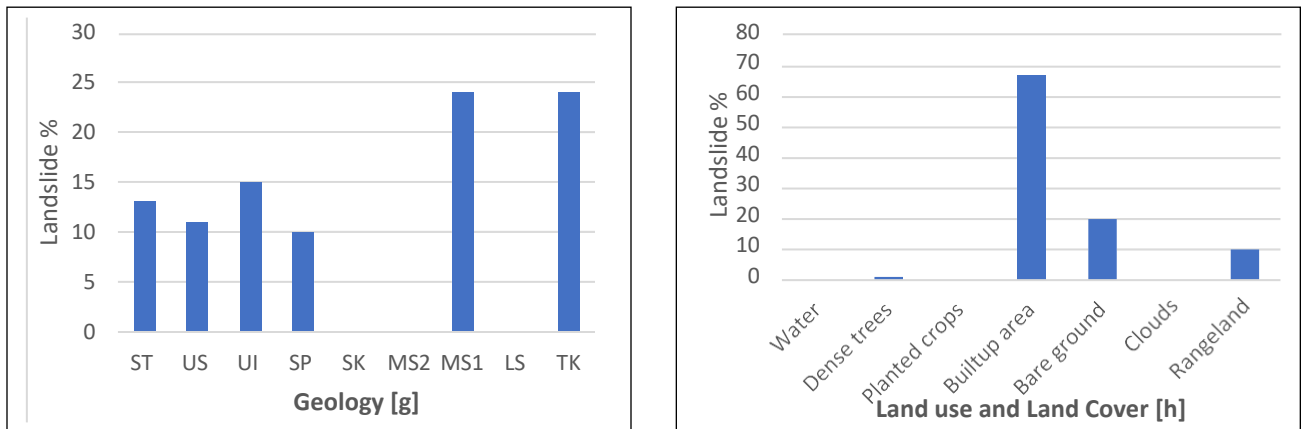


Figure 5: Relationship of landslides occurrences with the causative factors. (a) distance to stream (b) curvature, (c) aspect (d) slope (e) distance to road, (f) NDVI (g) geology, (h) LULC

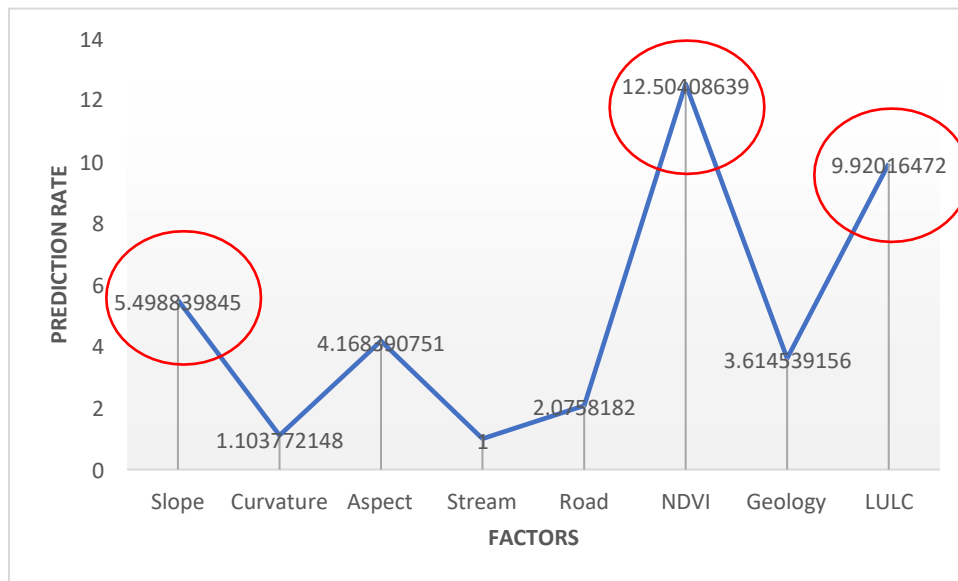


Figure 6: Different factors and their prediction rate for landslide susceptibility

Based on the analysis of the data, it has been found that NDVI (Normalized Difference Vegetation Index), LULC (Land Use Land Cover), and slope are the variables that have a higher prediction rate and weightage for the susceptibility of landslide. Therefore, incorporating these variables into landslide susceptibility models can improve their accuracy and reliability.

3.4 Landslide Susceptibility Map

To create an LSI map, the computed frequency ratios for the chosen classes of causative variables were integrated in GIS. For the purpose of creating a landslide susceptibility map for the research region, the LSI map is divided into five groups: very low, low, moderate, high, and very high susceptibility classes (Figure 7). According to the findings, the region has been classified into different susceptibility classes for landslides. Moderate class covers 24.6%, very low class covers 26.3%, and low susceptibility class covers 39.1% of the total area. High and extremely highly susceptible classes cover 7.7% and 2.08% of the total area, respectively.

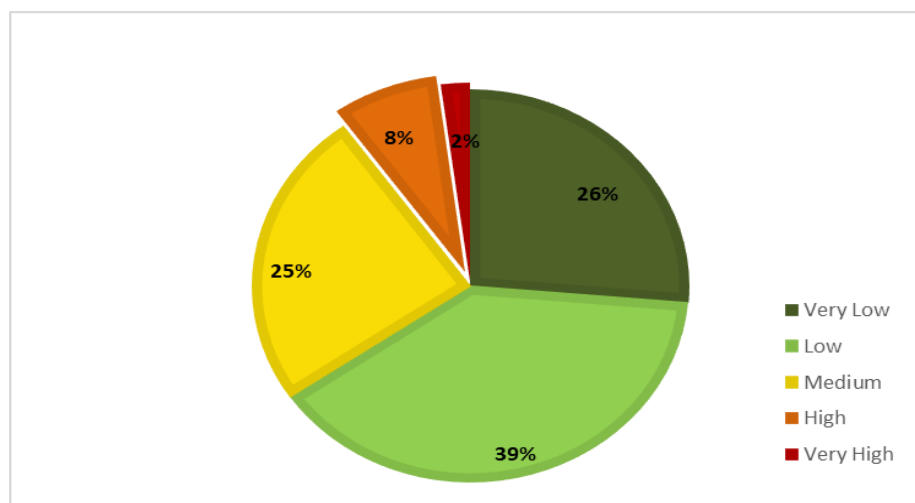


Figure 7: Distribution of landslides on different classes of susceptibility

For a landslide susceptibility study, a base map and a factor map are needed. The Landslide Inventory map served as the starting point. This research included both intrinsic and extrinsic characteristics, including slope, aspect, NDVI, geology, distance from roads, distance to streams, curvature, and land cover. The effectiveness and accessibility of the characteristics served as the sole criterion for selection. A combination between the landslide inventory map and factor map has been constructed in order to determine the frequency ratio (FR) for each class of the causative factors. Values higher than 1 indicate a higher correlation, while values lower than 1 indicate a lesser correlation, which suggests the proportion of the landslide is higher than the area. In order to create a landslide susceptibility map, the LSI map is classed.

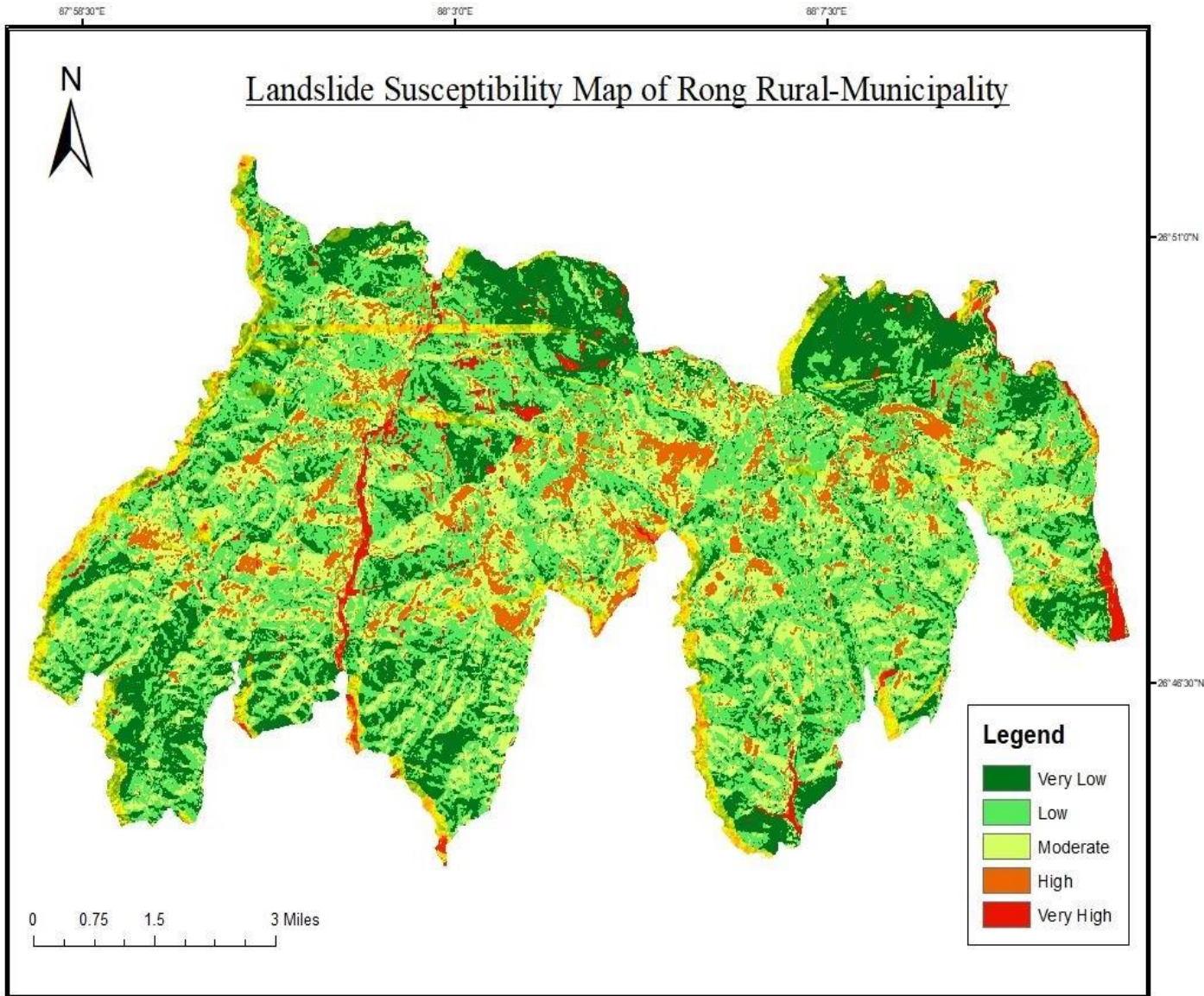


Figure 8: Landslide susceptibility map of Rong rural municipality

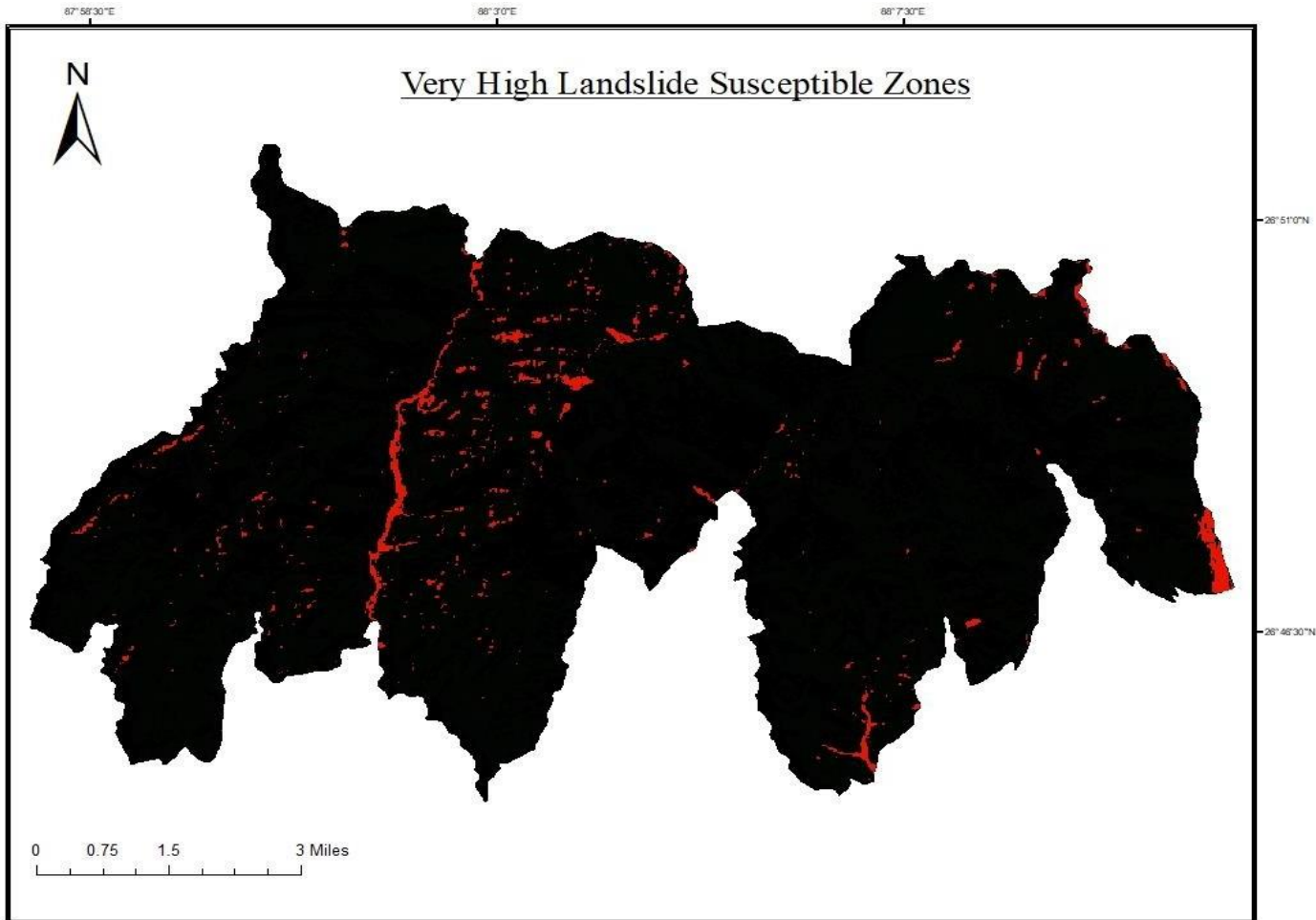


Figure 9: Very high Landslides Susceptible Zones

Based on the analysis conducted, it has been found that 2.08% of the total study area is categorized as being in the very high landslide susceptible zones. This area covers a total of 3.23 square kilometers, indicating the presence of a significant portion of the study area that is at a high risk of experiencing landslides. Annex 2 and Annex 3 have coordinates of very high susceptible and high susceptible zones of landslides respectively.

3.5 Discussion

The occurrence of the landslide in the Churia region of the rural municipality of Rong is caused by a number of factors. According to the study, the likelihood of a landslide increases as the slope angle rises. According to analysis, slopes with a higher degree of incline are more prone to landslides than slopes with a lower degree of incline. Gravitational pressure on the rocks and earth elements causes the bulk to collapse, resulting in a landslide, which is why susceptibility increases

as slope angle increases. Maximum landslides are discovered to occur in south-east and south-facing parts, according to the aspect map. The northern part of the hills has not had any landslides. The aspect (slope direction) influences how much sunlight, wind, and precipitation are exposed to an area, which indirectly impacts other landslide-causing elements including soil moisture, plant cover, and soil thickness. Land use and land cover data indicate that 67% of landslides occur in built up areas, whereas 20% occur in barren area. However, there were essentially no landslides in agricultural regions, water bodies, or places with forest cover. The occurrence of landslides depends on how far they are from a stream. According to analysis, there were 7% of landslides within the first 100 meters of the road, while at 500 and 1000 meters from the road, there were 21% and 20% landslides, respectively. The road network in the study region has the most impact on where landslides occur and how frequently they occur (Derbyshire et al., 2001).

The Churia region's young, delicate sedimentary strata have undergone extensive weathering and deformation. There are many possibilities for slope instability and the development of many types of landslides in these places because of the interbedding of soft mudstone and firm sandstone strata. Since the Siwalik or Churia region is mostly composed of mudstone, sandstone, and conglomerate, which increased the surface's sensitivity to hazards, geology largely governs the area's landslides. Data analysis reveals that Ulleri formation (UI) accounted for 15% of all landslides, with Takure formation (TK) and Lower middle siwalik (MS1) geology accounting for 24%. However, no landslides have yet happened in the geology of Sarung kh. Formation (Sk), Upper middle siwalik (MS2), and Lower siwalik (LS). According to the results of the field survey, landslides have a high reactivation rate, meaning that they can reactivate even after they have previously occurred. After examining the data, it was discovered that the least number of landslides were observed to occurred in more than 2500 meters away from the stream, but 21%, 24%, and 28% of landslides occurred in the first 100, 500, and 1000 meters from the stream, respectively. Landslides become less frequent when the distance from the stream is increased. Similarly, it was discovered that landslides were evenly distributed over the research area's curvature. According to NDVI data, landslides are most common in low NDVI area having the coverage of 86% of total landslides observed. Gradually landslide occurrence decreases to medium NDVI and high NDVI by 11% and 2% respectively. Most of the landslides that were observed during the field study had moderate weathering conditions, but some landslides were highly weathered, which may be related to the delicate geology of Churia, the variety of rock types in the region, and heavy monsoon

rainfall in the area may have causes significant soil surface erosion. The majority of shallow landslides, followed by erosional, debris slide, debris flow, and complicated landslides, are seen in the study region. Out of the total observed, landslides that were caused by erosion were mostly located along riverbanks. Uncertain rainfall patterns, weak geology, and river cutting may have been the main causes of landslides. While some of the landslides were discovered to be older, some of the landslides were believed to have been caused by road construction.

To lessen susceptibility and danger of loss of life and property, it is crucial to identify the locations that are most susceptible to landslides. As a result, a hazard susceptibility map using ArcGIS pro is created along with eight separate factor maps showing the distribution of landslides. The frequency ratio method's findings indicated that NDVI, geology, slope angle, and LULC are the main causes of landslides in the studied region

CHAPTER-IV: CONCLUSION

An essential tool for managing disasters, planning, mitigating damage, and averting risk in any given location is a map showing a region's susceptibility to landslides. For the purpose of forecasting potential landslides in a region, a map of landslide susceptibility is also created. In this work, remote sensing and GIS are efficiently employed to create an inventory of landslides, analyze their geographical distribution, and create a map of landslide susceptibility. The purpose of this study is to understand the current situation and forecast potential landslides in the Churia area of the Rong rural municipality. Frequency ratio approach was chosen from a variety of hazard assessment techniques because it is more appropriate, and best suited for the compact study region like Rong. Slope, aspect, land use, curvature, distance to road, distance to stream, geology, and NDVI were eight causal factors that were taken into account throughout the study. 105 landslides were discovered throughout the study, accounting for 0.30% of the overall studied area. NDVI, LULC, slope, and geology were discovered to be the main contributors to cause the landslides in the Churia area among the several components evaluated. 9.86% of the research area is characterized as susceptible to landslides (high and very high susceptible zones), according to the map of landslide susceptibility that was generated. In the research region, landslides have also been seen to be caused by anthropogenic activity.

Recommendations

Further geological and engineering study in the landslide susceptible zones is suggested for adopting appropriate mitigation and preventive measures. Landslides in Rong have significant history of causing physical and economic loss. The influence they may have cannot be ignored since landslides themselves exacerbate their effects on local residents' quality of life. Rong rural municipality should make every effort to deal with the local landslide issue.

Based on the present study following recommendations have been put forward.

- Implementing land-use planning and zoning regulations to restrict development in areas identified as high-risk for landslides.
- Developing early warning systems and emergency response plans to quickly identify and respond to potential landslides.
- Implementing structural measures such as retaining walls, drainage systems, and slope stabilization techniques to reduce the risk of landslides in high-risk areas.

- Educating the public and local officials about the risks of landslides and how to prepare for and respond to them.
- Monitoring and maintaining existing structures and infrastructure, such as roads and bridges, that may be impacted by landslides.
- Regularly updating the susceptibility map with new data and re-evaluate the management plans accordingly.

As the present study incorporates eight factors, further studies can be carried out incorporating the other triggering factors like fault zone, soil type, rainfall data etc.

REFERENCES

- Akgun, A., Serhat, D. S., & Bulut, F. (2007). Landslide susceptibility mapping for a landslide-prone area (Findikli, NE of Turkey) by likelihood-frequency ratio and weighted linear combination models. *Environ Geol*. doi:<http://dx.doi.org/10.1007/s00254-007-0882-8>
- Audisio, C., Nigrelli, G., & Lollino, G. (2009). A GIS tool for historical instability processes data entry: an approach to hazard management in two Italian Alpine River Basins. *Comput Geosci*, 1735–1747.
- Bhandari, B., & Dhakal, S. (2018). Lithological Control on Landslide in the BabaiKhola Watershed, Siwaliks Zone of Nepal. *American Journal of Earth Sciences*, V, 54-64.
- Bhandari, B., & Dhakal, S. (2019). Topographical and Geological Factors on Gully-Type Debris Flow in Malai River Catchment, Siwaliks, Nepal. *Journal of Nepal Geological Society*, 89-94.
- Derbyshire, E., Moniques, F., & Owen, L. (2001). Geomorphological Hazards along the Karakoram Highway: Khunjerab Pass to the Gilgit River, Northern Pakistan. *Erdkunde*, 49-71.
- Dhakal, S. (2014). Geological Divisions and Associated Hazards in Nepal. In U. R. Khadka, *Contemporary Environmental Issues and Methods in Nepal* (pp. 100-109). Kirtipur, Nepal: Central Department of Environmental Science, Tribhuvan University.
- Dhakal, S. (2015). Evolution of Geomorphologic Hazards in Hindu Kush Himalaya. In *Springer* (pp. 53-72). doi:https://doi.org/10.1007/978-4-431-55242-0_4
- Dhital, M. (2015). *Geology of the Nepal Himalaya: Regional Perspective of the Classic Collided Orogen*. Berlin: Springer.
- Dikau, R., Brunsten, D., Schrott, L., & Ibsen, M. (Eds.). (1996). *Landslide Recognition. Identification, Movement and Causes*. Chichester: Wiley & Sons.
- Fell, R., Corominas, J., Bonnard, C., Cascini, L., Leroi, E., & Savage, W. (2008). Guidelines for landslide susceptibility, hazard, and risk zoning for land use planning, joint technical committee (JTC-1) on landslides and engineered slopes. *Eng Geol* , 85-98.
- Gansser, A. (1964). *Geology of Himalayas*.

- Guzzetti, F., Carrara, A., Cardinali, M., & Reichenbach, P. (1999). Landslide hazard evaluation: a review of current techniques and their application in a multi-scale study, Central Italy. *Geomorphology* , 181-216.
- Lamichhane, S., & Bhattarai, D. (2019). Landslide Hazard Analysis by Using Arc GIS and Google Earth: A Case Study of Province 5, Nepal. *Trends Tech Sci Research*, III(4), 79-85.
- Lee, S., & Talib, J. (2005). Probabilistic landslide susceptibility and factor effect analysis. *Environ. Geol.* , 982-990.
- Lepore, C., Kamal, S., P, S., & Bras, R. (2011). Rainfall-induced landslide susceptibility zonation of Puerto Rico. *Environ Earth Sci, Springer-Verlag special issue*.
- Mandal, S., & Mondal, S. (2019). Probabilistic approaches and landslide susceptibility. Geoinformatics and modelling of landslide susceptibility and risk. environmental science and engineering. *Springer book series (ESE)*, 145.163.
- Mondal, & Maiti. (2013). Integrating the analytical hierarchy process (AHP) and the frequency ratio (FR) model in landslide susceptibility mapping of Shiv-khola watershed. *Int. J. of Dis. Risk Sci.*, 200-212.
- OCHA. (2020, July). *Nepal: FLOODS and Landslides*. Retrieved from Reliefweb: <https://reliefweb.int/disaster/fl-2020-000165-npl>
- Rossi, M., & Reichenbach, P. (2016). LAND-SE: a software for statistically based landslide susceptibility zonation, version 1.0. *Geosci Model Dev* , 3533–3543.
- Schuster, R. (1996). Socioeconomic significance of landslides. In A. Turner, & R. Schuster, *Landslides: investigation and mitigation: special report* (pp. 12-26). Washington DC: National Academic Press.
- Turner, A., & Schuster, R. (Eds.). (1996). *Landslides: investigation and mitigation: special report*. Washington DC: National Academic Press.
- Upreti, B. (1999). An Overview of the Stratigraphy and Tectonics of the Nepal Himalaya. *Journal of Asian Earth Sciences*, 577-606. doi:[https://doi.org/10.1016/S1367-9120\(99\)00047-4](https://doi.org/10.1016/S1367-9120(99)00047-4)
- Varnes, D. (1996). *Landslide Hazard Zonation: A Review of Principles and Practice*. Paris, France: UNESCO.

- Yalcin, A. (2008). GIS-based landslide susceptibility mapping using analytical hierarchy process and bivariate statistic in Ardesen (Turkey): comparison of results and confirmations. *CATENA*, 1–12.
- Yalcin, A., Reis, S., Aydinoglu, A., & Yomralioglu, T. (2011). AGIS-based comparative study of frequency ratio, analytical hierarchy process, bivariate statistical and logistics regression methods for landslide susceptibility mapping in Trabzon. *Catena*, 274-287.
- Yilmaz, I. (2009). Landslide susceptibility mapping using frequency ratio, logistic regression, artificial neural networks and their comparison: a case study from Kat landslides (Tokat-Turkey). *Comput Geosci*, 1125-1138.
- Yilmaz, I., & Keskin, I. (2009). GIS based statistical and physical approaches to landslide susceptibility mapping (Sebinkarahisar, Turkey). *Bull Eng Geol Environ*, 459-471.

ANNEXES

Annex 1: Landslide inventory co-ordinate

FID	Polygon	Easting	Northing
0	Landslide 0	88° 3' 19.892" E	26° 45' 22.331" N
1	Landslide 1	88° 6' 34.301" E	26° 45' 25.564" N
2	Landslide 2	88° 2' 32.958" E	26° 45' 37.151" N
3	Landslide 3	88° 6' 14.583" E	26° 45' 37.655" N
4	Landslide 4	87° 59' 15.071" E	26° 45' 38.893" N
5	Landslide 5	88° 7' 33.739" E	26° 45' 44.408" N
6	Landslide 6	88° 7' 34.587" E	26° 45' 47.607" N
7	Landslide 7	88° 2' 16.223" E	26° 45' 55.852" N
8	Landslide 8	88° 7' 30.893" E	26° 45' 53.734" N
9	Landslide 9	88° 2' 1.196" E	26° 45' 59.008" N
10	Landslide 10	88° 2' 19.069" E	26° 46' 0.101" N
11	Landslide 11	88° 2' 5.411" E	26° 46' 6.288" N
12	Landslide 12	88° 2' 10.124" E	26° 46' 9.425" N
13	Landslide 13	88° 2' 39.547" E	26° 46' 20.237" N
14	Landslide 14	88° 1' 53.319" E	26° 46' 20.248" N
15	Landslide 15	88° 2' 30.058" E	26° 46' 31.119" N
16	Landslide 16	88° 2' 48.994" E	26° 46' 31.638" N
17	Landslide 17	88° 2' 6.000" E	26° 46' 32.688" N
18	Landslide 18	88° 8' 45.783" E	26° 46' 33.832" N
19	Landslide 19	88° 2' 28.139" E	26° 46' 36.510" N
20	Landslide 20	88° 8' 8.602" E	26° 46' 37.226" N
21	Landslide 21	88° 0' 54.021" E	26° 46' 47.543" N
22	Landslide 22	88° 8' 39.330" E	26° 46' 49.610" N
23	Landslide 23	88° 8' 43.019" E	26° 46' 45.407" N
24	Landslide 24	88° 3' 31.145" E	26° 46' 50.970" N
25	Landslide 25	88° 2' 14.283" E	26° 46' 55.206" N
26	Landslide 26	88° 7' 16.614" E	26° 46' 58.814" N
27	Landslide 27	87° 59' 52.043" E	26° 46' 59.691" N
28	Landslide 28	88° 2' 13.061" E	26° 47' 0.632" N
29	Landslide 29	87° 59' 55.269" E	26° 46' 59.505" N
30	Landslide 30	88° 7' 2.546" E	26° 47' 6.052" N
31	Landslide 31	88° 1' 56.584" E	26° 47' 5.542" N
32	Landslide 32	88° 7' 3.227" E	26° 47' 6.601" N
33	Landslide 33	88° 6' 53.066" E	26° 47' 8.211" N
34	Landslide 34	88° 2' 13.179" E	26° 47' 7.259" N
35	Landslide 35	88° 2' 47.426" E	26° 47' 8.528" N
36	Landslide 36	88° 2' 9.836" E	26° 47' 8.800" N
37	Landslide 37	88° 0' 32.932" E	26° 47' 8.549" N

38	Landslide 38	88° 2' 41.475" E	26° 47' 9.725" N
39	Landslide 39	88° 0' 0.911" E	26° 47' 9.805" N
40	Landslide 40	88° 7' 8.937" E	26° 47' 12.571" N
41	Landslide 41	88° 2' 16.571" E	26° 47' 15.217" N
42	Landslide 42	88° 2' 23.127" E	26° 47' 20.792" N
43	Landslide 43	88° 2' 10.568" E	26° 47' 22.175" N
44	Landslide 44	88° 9' 53.328" E	26° 47' 24.180" N
45	Landslide 45	88° 2' 28.878" E	26° 47' 20.750" N
46	Landslide 46	88° 9' 54.101" E	26° 47' 24.878" N
47	Landslide 47	87° 58' 40.962" E	26° 47' 26.623" N
48	Landslide 48	87° 58' 41.150" E	26° 47' 26.038" N
49	Landslide 49	88° 10' 3.635" E	26° 47' 27.752" N
50	Landslide 50	88° 0' 13.597" E	26° 47' 27.527" N
51	Landslide 51	88° 2' 45.508" E	26° 47' 28.082" N
52	Landslide 52	88° 0' 21.518" E	26° 47' 28.132" N
53	Landslide 53	88° 0' 24.311" E	26° 47' 29.601" N
54	Landslide 54	88° 9' 54.897" E	26° 47' 31.785" N
55	Landslide 55	87° 59' 11.262" E	26° 47' 35.974" N
56	Landslide 56	88° 2' 47.182" E	26° 47' 36.575" N
57	Landslide 57	88° 4' 36.054" E	26° 47' 37.366" N
58	Landslide 58	87° 59' 49.004" E	26° 47' 36.486" N
59	Landslide 59	88° 1' 6.489" E	26° 47' 38.735" N
60	Landslide 60	88° 10' 3.924" E	26° 47' 38.658" N
61	Landslide 61	88° 2' 55.142" E	26° 47' 39.549" N
62	Landslide 62	88° 0' 45.762" E	26° 47' 41.179" N
63	Landslide 63	88° 10' 28.139" E	26° 47' 41.692" N
64	Landslide 64	88° 9' 58.669" E	26° 47' 43.576" N
65	Landslide 65	88° 0' 47.606" E	26° 47' 43.225" N
66	Landslide 66	88° 10' 30.577" E	26° 47' 46.165" N
67	Landslide 67	88° 0' 38.396" E	26° 47' 47.233" N
68	Landslide 68	88° 0' 52.481" E	26° 48' 1.406" N
69	Landslide 69	88° 5' 15.674" E	26° 48' 0.090" N
70	Landslide 70	87° 59' 55.396" E	26° 48' 9.638" N
71	Landslide 71	88° 10' 5.626" E	26° 48' 16.356" N
72	Landslide 72	88° 10' 8.301" E	26° 48' 19.144" N
73	Landslide 73	88° 5' 17.561" E	26° 48' 31.386" N
74	Landslide 74	88° 6' 56.124" E	26° 48' 36.304" N
75	Landslide 75	88° 4' 39.626" E	26° 48' 44.642" N
76	Landslide 76	88° 4' 3.465" E	26° 48' 47.352" N
77	Landslide 77	88° 6' 50.491" E	26° 48' 50.950" N
78	Landslide 78	88° 5' 26.468" E	26° 48' 49.949" N
79	Landslide 79	88° 4' 51.749" E	26° 48' 53.225" N

80	Landslide 80	88° 9' 2.794" E	26° 48' 57.529" N
81	Landslide 81	88° 9' 1.926" E	26° 48' 59.259" N
82	Landslide 82	88° 3' 52.851" E	26° 48' 59.775" N
83	Landslide 83	88° 4' 41.755" E	26° 49' 4.927" N
84	Landslide 84	88° 8' 41.441" E	26° 49' 4.644" N
85	Landslide 85	88° 8' 28.480" E	26° 49' 5.345" N
86	Landslide 86	88° 4' 49.963" E	26° 49' 8.946" N
87	Landslide 87	88° 4' 20.062" E	26° 49' 10.324" N
88	Landslide 88	88° 4' 41.688" E	26° 49' 15.119" N
89	Landslide 89	88° 4' 43.827" E	26° 49' 16.926" N
90	Landslide 90	88° 6' 53.719" E	26° 49' 22.426" N
91	Landslide 91	88° 3' 7.694" E	26° 49' 31.222" N
92	Landslide 92	88° 3' 7.637" E	26° 49' 30.765" N
93	Landslide 93	88° 1' 53.759" E	26° 49' 40.494" N
94	Landslide 94	88° 9' 19.758" E	26° 49' 43.100" N
95	Landslide 95	88° 2' 44.003" E	26° 49' 49.757" N
96	Landslide 96	88° 9' 16.303" E	26° 49' 55.846" N
97	Landslide 97	88° 2' 26.216" E	26° 49' 59.703" N
98	Landslide 98	88° 3' 20.320" E	26° 50' 5.329" N
99	Landslide 99	88° 1' 12.239" E	26° 50' 8.191" N
100	Landslide 100	88° 1' 47.123" E	26° 50' 15.692" N
101	Landslide 101	88° 1' 58.715" E	26° 50' 19.617" N
102	Landslide 102	88° 2' 4.505" E	26° 50' 20.879" N
103	Landslide 103	88° 8' 16.006" E	26° 50' 30.812" N
104	Landslide 104	88° 1' 34.677" E	26° 50' 31.543" N

Annex 2: Very high susceptible landslide zones co-ordinate

FID	Shape *	Easting	Northing
0	Point 0	88° 3' 51.186" E	26° 49' 15.362" N
1	Point 1	88° 4' 20.228" E	26° 49' 46.099" N
2	Point 2	88° 4' 29.910" E	26° 49' 56.345" N
3	Point 3	88° 4' 46.106" E	26° 49' 45.903" N
4	Point 4	88° 3' 8.346" E	26° 49' 46.639" N
5	Point 5	88° 3' 16.717" E	26° 49' 19.060" N
6	Point 6	88° 3' 43.375" E	26° 48' 59.942" N
7	Point 7	88° 3' 24.041" E	26° 48' 42.029" N
8	Point 8	88° 2' 54.755" E	26° 47' 43.772" N
9	Point 9	88° 2' 51.975" E	26° 47' 54.112" N
10	Point 10	88° 2' 10.352" E	26° 47' 7.983" N
11	Point 11	88° 2' 52.128" E	26° 46' 26.400" N
12	Point 12	88° 0' 51.729" E	26° 47' 1.673" N

13	Point 13	87° 58' 47.747" E	26° 46' 16.969" N
14	Point 14	87° 58' 24.532" E	26° 47' 43.122" N
15	Point 15	88° 0' 8.964" E	26° 47' 41.533" N
16	Point 16	87° 59' 52.577" E	26° 47' 30.470" N
17	Point 17	87° 59' 16.727" E	26° 48' 35.216" N
18	Point 18	87° 59' 33.070" E	26° 48' 41.121" N
19	Point 19	88° 1' 18.666" E	26° 50' 47.637" N
20	Point 20	88° 2' 44.804" E	26° 50' 32.389" N
21	Point 21	88° 4' 0.391" E	26° 50' 17.206" N
22	Point 22	88° 4' 58.876" E	26° 50' 18.481" N
23	Point 23	88° 4' 38.050" E	26° 50' 46.157" N
24	Point 24	88° 4' 40.518" E	26° 50' 3.143" N
25	Point 25	88° 3' 25.510" E	26° 49' 37.052" N
26	Point 26	88° 3' 14.896" E	26° 49' 29.392" N
27	Point 27	88° 2' 33.661" E	26° 49' 27.118" N
28	Point 28	88° 1' 17.785" E	26° 50' 56.242" N
29	Point 29	87° 58' 43.865" E	26° 48' 2.767" N
30	Point 30	88° 1' 41.238" E	26° 46' 26.919" N
31	Point 31	88° 0' 34.157" E	26° 46' 24.821" N
32	Point 32	88° 1' 39.880" E	26° 47' 28.843" N
33	Point 33	88° 1' 54.485" E	26° 47' 54.534" N
34	Point 34	88° 2' 15.068" E	26° 48' 45.119" N
35	Point 35	88° 2' 13.355" E	26° 49' 7.489" N
36	Point 36	88° 2' 45.963" E	26° 49' 9.829" N
37	Point 37	88° 2' 30.503" E	26° 48' 56.184" N
38	Point 38	88° 1' 58.006" E	26° 49' 5.881" N
39	Point 39	88° 2' 46.555" E	26° 50' 14.318" N
40	Point 40	88° 6' 6.998" E	26° 48' 45.946" N
41	Point 41	88° 6' 40.393" E	26° 45' 14.148" N
42	Point 42	88° 7' 2.775" E	26° 45' 50.088" N
43	Point 43	88° 8' 2.521" E	26° 49' 38.347" N
44	Point 44	88° 8' 12.499" E	26° 50' 17.822" N
45	Point 45	88° 9' 22.398" E	26° 50' 10.376" N
46	Point 46	88° 8' 44.577" E	26° 49' 26.829" N
47	Point 47	88° 8' 57.968" E	26° 49' 24.141" N
48	Point 48	88° 10' 31.770" E	26° 49' 12.192" N
49	Point 49	88° 10' 50.630" E	26° 47' 9.931" N
50	Point 50	88° 10' 47.952" E	26° 47' 28.870" N
51	Point 51	88° 8' 55.488" E	26° 48' 28.268" N
52	Point 52	88° 6' 10.539" E	26° 48' 15.821" N
53	Point 53	88° 8' 11.237" E	26° 46' 35.118" N
54	Point 54	88° 7' 2.590" E	26° 45' 31.172" N

55	Point 55	88° 7' 27.807" E	26° 46' 2.789" N
56	Point 56	88° 7' 31.452" E	26° 45' 43.842" N
57	Point 57	88° 4' 11.651" E	26° 49' 51.324" N
58	Point 58	88° 3' 42.601" E	26° 49' 19.726" N
59	Point 59	88° 3' 38.856" E	26° 49' 29.213" N
60	Point 60	88° 0' 18.742" E	26° 48' 3.822" N
61	Point 61	88° 0' 52.096" E	26° 47' 42.946" N
62	Point 62	88° 7' 59.859" E	26° 49' 59.866" N
63	Point 63	88° 1' 47.208" E	26° 48' 37.583" N
64	Point 64	88° 1' 56.510" E	26° 48' 6.558" N
65	Point 65	88° 2' 0.031" E	26° 47' 32.136" N
66	Point 66	88° 4' 37.211" E	26° 47' 36.124" N

Annex 3: High susceptible landslide zones co-ordinate

FID	Shape *	X	Y
0	Point 0	88° 6' 29.309" E	26° 45' 56.370" N
1	Point 1	88° 3' 35.652" E	26° 47' 10.791" N
2	Point 2	88° 3' 24.338" E	26° 47' 30.654" N
3	Point 3	88° 3' 18.733" E	26° 47' 46.174" N
4	Point 4	88° 4' 17.648" E	26° 48' 35.606" N
5	Point 5	88° 4' 26.370" E	26° 48' 45.859" N
6	Point 6	88° 4' 27.507" E	26° 49' 4.769" N
7	Point 7	88° 5' 20.173" E	26° 49' 0.067" N
8	Point 8	88° 5' 46.948" E	26° 48' 53.840" N
9	Point 9	88° 5' 31.418" E	26° 48' 33.323" N
10	Point 10	88° 6' 49.859" E	26° 48' 18.953" N
11	Point 11	88° 6' 22.804" E	26° 47' 55.948" N
12	Point 12	88° 6' 39.917" E	26° 47' 42.056" N
13	Point 13	88° 6' 1.451" E	26° 47' 27.737" N
14	Point 14	88° 8' 4.736" E	26° 48' 32.117" N
15	Point 15	88° 8' 52.968" E	26° 49' 3.544" N
16	Point 16	88° 8' 14.756" E	26° 49' 15.891" N
17	Point 17	88° 7' 32.165" E	26° 48' 33.237" N
18	Point 18	88° 6' 36.771" E	26° 48' 52.592" N
19	Point 19	88° 6' 40.898" E	26° 49' 22.656" N
20	Point 20	88° 6' 18.856" E	26° 49' 22.829" N
21	Point 21	88° 5' 56.830" E	26° 49' 24.720" N
22	Point 22	88° 1' 56.947" E	26° 47' 8.941" N
23	Point 23	88° 1' 26.659" E	26° 47' 50.437" N
24	Point 24	88° 1' 17.720" E	26° 47' 15.244" N
25	Point 25	88° 0' 25.306" E	26° 47' 47.437" N

26	Point 26	88° 0' 21.321" E	26° 47' 30.267" N
27	Point 27	87° 59' 38.235" E	26° 47' 34.011" N
28	Point 28	87° 59' 10.717" E	26° 48' 5.160" N
29	Point 29	88° 0' 30.659" E	26° 48' 51.033" N
30	Point 30	88° 1' 14.434" E	26° 48' 16.322" N
31	Point 31	88° 1' 23.212" E	26° 48' 33.457" N
32	Point 32	88° 1' 35.809" E	26° 48' 48.845" N
33	Point 33	88° 0' 46.076" E	26° 49' 0.382" N
34	Point 34	88° 1' 5.381" E	26° 49' 15.722" N
35	Point 35	88° 1' 21.627" E	26° 49' 10.445" N
36	Point 36	88° 1' 46.537" E	26° 49' 9.405" N
37	Point 37	88° 1' 33.267" E	26° 49' 25.839" N
38	Point 38	88° 1' 49.638" E	26° 49' 34.320" N
39	Point 39	88° 2' 12.663" E	26° 49' 36.731" N
40	Point 40	88° 1' 59.643" E	26° 50' 20.682" N
41	Point 41	88° 1' 30.957" E	26° 50' 28.630" N
42	Point 42	88° 2' 5.699" E	26° 50' 54.174" N
43	Point 43	88° 5' 30.665" E	26° 48' 54.826" N
44	Point 44	88° 4' 52.427" E	26° 47' 23.970" N
45	Point 45	88° 5' 1.483" E	26° 48' 9.475" N
46	Point 46	88° 5' 11.933" E	26° 47' 59.936" N
47	Point 47	88° 4' 48.158" E	26° 48' 19.036" N
48	Point 48	88° 5' 26.396" E	26° 48' 9.284" N
49	Point 49	88° 3' 48.006" E	26° 48' 42.709" N
50	Point 50	88° 6' 52.247" E	26° 47' 29.060" N
51	Point 51	88° 8' 19.081" E	26° 46' 53.113" N
52	Point 52	88° 8' 38.637" E	26° 49' 7.960" N
53	Point 53	88° 0' 38.421" E	26° 50' 49.646" N
54	Point 54	88° 0' 47.301" E	26° 51' 17.960" N
55	Point 55	88° 10' 10.632" E	26° 47' 42.938" N
56	Point 56	88° 9' 6.089" E	26° 48' 43.660" N
57	Point 57	88° 9' 11.167" E	26° 49' 11.995" N
58	Point 58	88° 9' 25.673" E	26° 49' 24.775" N
59	Point 59	88° 9' 0.878" E	26° 49' 37.016" N
60	Point 60	88° 9' 23.374" E	26° 50' 21.547" N